Integrated Optical Link on Si Substrate Using Membrane Distributed-Feedback Laser and p-i-n Photodiode

Daisuke Inoue, *Student Member, IEEE*, Takuo Hiratani, *Student Member, IEEE*, Kai Fukuda, Takahiro Tomiyasu, Zhichen Gu, Tomohiro Amemiya, *Member, IEEE*, Nobuhiko Nishiyama, *Senior Member, IEEE*, and Shigehisa Arai, *Fellow, IEEE*

***Abstract*—On-chip optical interconnection is a promising technology for wiring future large-scale integrated circuits, as a means to mitigate the considerable power dissipation of traditional wiring layers. Here, we fabricate an integrated optical link using a membrane distributed-feedback (DFB) laser and a p-i-n photodiode (PD) in a butt-jointed built-in coupling geometry. The optical link is formed on a Si substrate by benzocyclobutene bonding. The integrated DFB laser shows a low-threshold current of 0.48 mA. Light transmission between the DFB laser and the p-i-n PD is confirmed with static measurements of the optical link. The optical link has a 3-dB bandwidth of 11.3 GHz at a 2.73 mA DFB laser bias current and a –3 V p-i-n PD bias voltage. A data transmission experiment of the optical link is performed, using a nonreturn to zero, pseudorandom-bit-sequence with a word length of 2^{31}-1 signals. With a DFB laser bias current of 2.5 mA, 10 Gbit/s data transmission with a bit-error-rate of 6×10^{-7} is successfully achieved.**

***Index Terms*—Distributed-feedback laser, lateral current injection, membrane laser, optical interconnection, semiconductor laser.**

I. Introduction

THE wiring layer of large-scale integrated circuits is responsible for a large fraction of the total chip power dissipation [1]–[3]. To mitigate this problem, new interconnection technology is required. Novel type on-chip electrical interconnection technologies such as carbon-nanotubes [4] and high-speed transmission lines [5]–[7] have been proposed as approaches capable of achieving energy efficient wiring with small transmission delays. On-chip optical interconnection—in contrast with electrical approaches—has also been recognized as a promising candidate for future wiring schemes [8]–[10]. As in fiber optic communications, on-chip optical interconnection consists of light sources, passive waveguides, and detectors. There are two main approaches to implement on-chip optical links: on-chip light sources, and external light sources with on-chip modulators. As an external light source approach, on-chip optical links have been demonstrated on silicon photonic platforms with an external laser and ring modulators [11]–[14]. Although silicon ring modulators can operate at high-speed and with low-energy consumption, they require heater tuning to change their operation wavelength to that of the external laser [14], because the operation wavelength of the ring modulator is easily affected by temperature changes and fabrication tolerances. Even though the energy consumption of the ring modulator is itself very small (several fJ/bit [15]), that of micro-heaters is much higher than that, and has been reported to be as high as 192 fJ/bit [14]. An optical link implemented on a III-V/silicon-on-insulator (III-V/SOI) platform using an electro-absorption modulator achieved high-speed operation with a 3-dB bandwidth of 13 GHz [16]. A twin-guide laser and a uni-carrier travelling photodiode integrated with InP-membrane circuit were demonstrated [17]. By employing a directly modulated on-chip light source, a reduction of the laser current results in a reduction in the total consumed link energy. A key challenge concerning on-chip light sources is to obtain ultra-low energy consumption semiconductor lasers [18]. Vertical-cavity surface-emitting lasers (VCSELs) can operate with low-threshold and high-speed direct modulation [19], [20]. The VCSEL structure is suitable for vertical fiber coupling (rather than horizontal integration) and requires a 45° total reflection mirror to make an in-plane optical link [21]. Ring lasers [22] and microdisk lasers [23], [24] have been used in III-V/SOI optical links. Even though these lasers are capable of low-threshold and high-speeds, the evanescent coupling between the laser and the passive waveguide prevents an efficient light coupling. Photonic crystal lasers exhibited 4.8-μA threshold operation [25], and optical links using photonic crystal waveguides and p-i-n photodiodes (PDs) have been demonstrated [26]. Ultra-low energy signal transmission was reported, but the transmitted signal of this optical link structure (laser and PD integration) was not evaluated in terms of

Manuscript received January 22, 2017; revised May 3, 2017 and June 9, 2017; accepted June 10, 2017. This work was supported by the Japan Society for the Promotion of Science KAKENHI under Grant 15H05763, Grant 25709026, Grant 15J04654, Grant 15J11776, and Grant 16H06082, and by JST-CREST. *(Corresponding author: Daisuke Inoue.)*

D. Inoue, T. Hiratani, K. Fukuda, T. Tomiyasu, and Z. Gu are with the Department of Electrical and Electronic Engineering, Tokyo Institute of Technology, Tokyo 152-8552, Japan (e-mail: inoue.d.ac@m.titech.ac.jp; hiratani.t@gmail.com; fukuda.k.an@m.titech.ac.jp; tomiyasu.t.aa@m.titech.ac.jp; gu.z.ab@m.titech.ac.jp).

T. Amemiya, N. Nishiyama, and S. Arai are with the Institute of Innovative Research, Tokyo Institute of Technology, Tokyo 152-8552, Japan (e-mail: amemiya.t.ab@m.titech.ac.jp; n-nishi@pe.titech.ac.jp; arai@pe.titech.ac.jp).

Color versions of one or more of the figures in this paper are available online at http://ieeexplore.ieee.org.

Digital Object Identifier 10.1109/JSTQE.2017.2716184

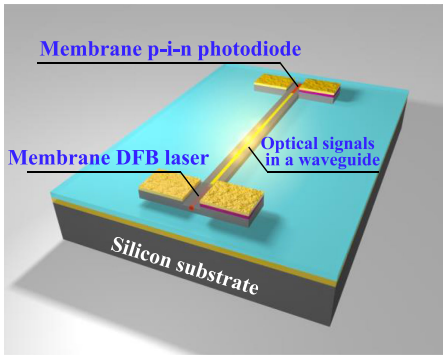

Fig. 1. Schematic of a membrane optical link on a silicon substrate.

bit-error-rate characteristics, because of the small output power of the photonic crystal laser.

As discussed above, on-chip optical interconnections require low-power consumption lasers and efficient coupling structures. Membrane distributed-feedback (DFB) lasers—DFB lasers fabricated in thin semiconductor layers—are promising candidates as light sources for on-chip optical interconnection [27]. A schematic of an optical link using a membrane DFB laser is shown in Fig. 1. The edge-emitting structure of the DFB laser is well suited for in-plane integration, and is widely used as the light source in photonic integrated circuits [28], [29]. The typical operating current of DFB lasers is of several tens of milliamperes due to its large active volume [30], [31]. The membrane structure has an ability to reduce the operating current of DFB laser as following reasons. A thin semiconductor layer sandwiched by dielectric claddings enhances the optical confinement factor of the active layers [32]. A large refractive-index difference between the core and cladding layers results in strong grating index-coupling [33]. These properties make the membrane DFB laser a candidate for use as a low-power consumption light source [34]. In our early works, optically pumped operation has revealed low-threshold and strong index-coupled characteristics [35]–[37]. By adopting a lateral-current-injection (LCI) structure [38]–[41], LCI-membrane lasers were operated with both pulsed [42] and continuous-waves (CWs) [43], [44]. Many integration schemes are available, such as butt-jointed built-in (BJB) structures [45], quantum-well intermixing [46], offset quantum wells [47], and so on. We adopted a BJB structure to integrate the membrane DFB laser with a passive waveguide section [48]; a low threshold current of 0.23 mA was achieved with the BJB waveguide [49]. Integration with a distributed-Bragg reflector enhanced the output efficiency [50]. Recent works showed the high speed modulation properties of membrane DFB lasers at low-bias currents [51], [52]. Optical transmission has been performed using monolithically integrated membrane DFB lasers and p-i-n PDs [53]. However, the dynamic characteristics of the membrane optical link have not hitherto been investigated.

In this paper, we fabricated an integrated optical link consisting of a membrane DFB laser, a p-i-n PD, and a passive waveguide. Fabrication procedure of the membrane optical link is shown in Section II. The static characteristics of the optical link are characterized in Section III. The small-signal modulation measurements are performed in Section IV. Finally, a large-signal data transmission through the optical link is presented in Section V.

II. Membrane Optical Link Fabrication Procedure

A membrane optical link was fabricated by three-step organometallic vapor-phase-epitaxy (OMVPE) regrowth and benzocyclobutene (BCB) adhesive bonding. The detailed process is described in [49]. The initial wafer consisted of a 270-nm-thick core layer including a five-quantum-well (5QW) active layer, a p^{++}-GaInAs contact layer, and sacrificial etch stop layers. The active region had a photoluminescence peak at a wavelength of 1520 nm. The fabrication was started with the three-step OMVPE regrowth. First, a passive GaInAsP waveguide layer was regrown. The fabrication procedure for BJB structure of the active and passive sections was described in [53]. Subsequently, n-InP and p-InP layers were regrown, for the lateral p-i-n diode structure. A SiO_2 cladding layer was deposited on the regrown InP substrate by a plasma-enhanced chemical vapor deposition. After BCB adhesive bonding of the initial wafer onto a silicon substrate, the InP substrate was removed by chemical polishing and selective wet chemical etching. Au/Zn/Au (25/50/300 nm) was deposited as the p-side electrode by thermal evaporation, and annealed at 350 °C in N_2 ambient for one minute. Ti/Au (25/200 nm) was then deposited on both n-side and p-side electrode regions by electron beam evaporation. A surface grating pattern was defined by electron beam lithography. The grating design was uniform first order grating with period of 295 nm and duty ratio of 0.43. The pattern formed on a SiO_2 mask was transferred to an InP cap layer by wet chemical etching. The etching for 50-nm-depth grating was performed using chemical etchant of H_2O: H_2O_2: HCl: $CH_3COOH = 92$: 1: 2: 20 at 10 °C for 8 s. The etching rate for an InP was approximately 6 nm/s. Finally, stripe-shaped photoresist for protecting both an active and a passive waveguide region was formed by photolithography. The unnecessary InP region was then removed by wet chemical etching, to enhance the electrical isolation between the devices. Fig. 2(a) shows an optical microscopy image of the fabricated membrane optical link and cross-sections at the active and passive regions. The DFB laser and the p-i-n PD had lengths of 80 and 200 μm, respectively. The absorption layer of the p-i-n PD was the same as that of the active region of the DFB laser. These devices were connected by a 500-μm-long passive waveguide. The coupling efficiency between the active and passive section was calculated to be 98% [48]. The propagation loss of the passive waveguide was measured to be more than 8 dB/cm by the Fabry-Perot resonance method using the waveguide with both cleaved facets. The propagation loss for a 500-μm-long waveguide was at least 0.4 dB. The output of the DFB laser on the opposite side to the p-i-n PD was cleaved, for measuring the lasing characteristics. Fig. 2(b) shows a scanning electron microscopy image of the DFB laser region. As shown, the surface grating pattern was successfully formed on the InP cap layer. The electrical isolation between the DFB laser and the p-i-n PD is important to ensure independent device driving and to suppress crosstalk in

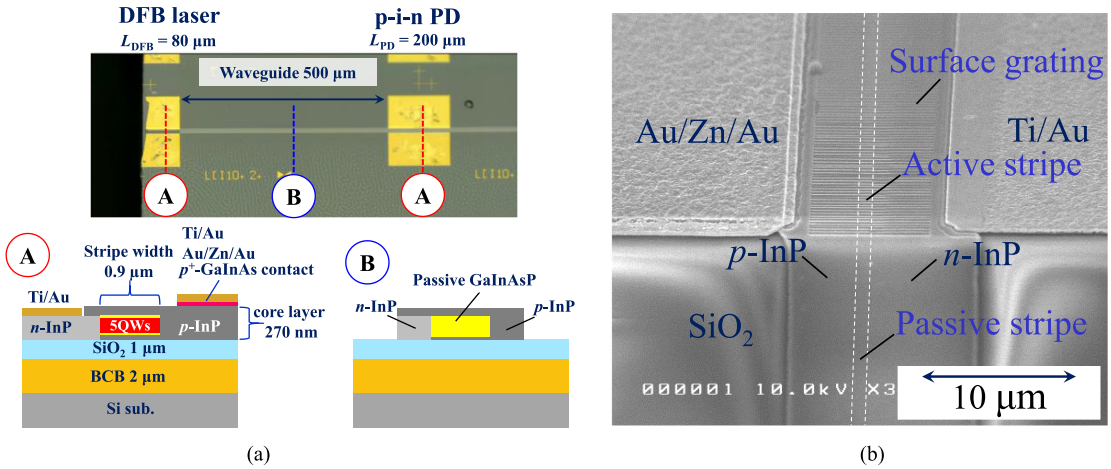

Fig. 2. (a) Optical microscopy image and cross sections of the optical link fabricated using a membrane DFB laser and a p-i-n PD. (b) Scanning electron microscopy image of a joint region of the DFB laser and the passive waveguide.

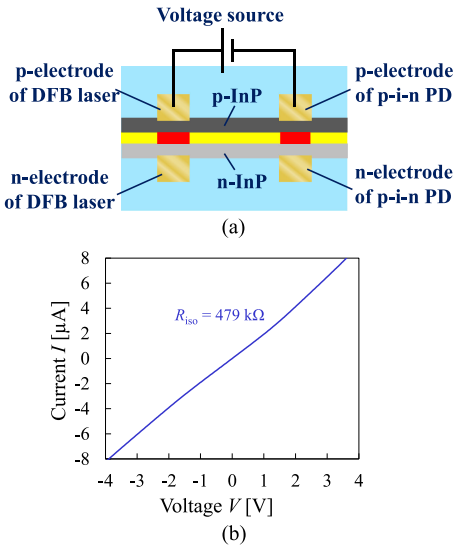

Fig. 3. Electrical isolation measurement. (a) Schematic of the measuring configuration. (b) Current–voltage characteristics.

the integrated structure. The electrical isolation resistance $R_{\rm iso}$ between the p-side electrodes of the DFB laser and the p-i-n PD was measured, as shown in Fig. 3(a). Given that the n-electrodes will be set to common ground during the optical transmission measurement, the isolation resistance between the n-side electrodes becomes not a serious problem. Fig. 3(b) shows the obtained current–voltage characteristics. The isolation resistance $R_{\rm iso}$ was measured to be of approximately 479 kΩ; at the device operating voltage, the leakage current was therefore expected to be under 10 μA, which implies that sufficient electrical isolation was obtained in the fabricated structure.

III. Static Characteristics

Prior to evaluating the fabricated optical link, the static characteristics of the integrated membrane DFB laser were measured. The DFB laser was characterized by measuring the light output from the cleaved facet formed on the side opposite to the p-i-n PD. The light output was detected by a commercial p-i-n PD. Fig. 4(a) shows the light output versus current and the applied voltage versus current characteristics. The obtained threshold current $I_{\rm th}$ was 0.48 mA, and the corresponding threshold current density $J_{\rm th}$ was 667 A/cm^2 for the 5QW active layer. The external differential quantum efficiency $\eta_{\rm d}$ was 2.5% (facet output). It should be noted that even though the output efficiency from the facet was small, the facet output was not used in the optical transmission measurement to be shown later. Fig. 4(b) shows the lasing spectrum measured at a bias current of 2.5 mA; in these measurements, the lasing wavelength was 1525 nm and the sub-mode suppression-ratio was 34 dB. The stopband width— which can be defined as the wavelength range with very low intensity level—was 43 nm, corresponding to an index-coupling coefficient of 2000 cm^{-1}. Same values of stopband width were observed for the different devices on a same chip. The slight difference of Bragg wavelength was observed between the devices, which was attributed to the variation of stripe width or non-uniformity of regrowth thickness. Fig. 4(c) shows input power versus lasing wavelength characteristics. The slope $\Delta\lambda/\Delta P_{\rm in}$ was 0.226 nm/mW.

The optical link was then statically characterized, by measuring the optical transmission properties between the DFB laser and the p-i-n PD. The light output of the DFB laser into the passive waveguide section was detected by the integrated p-i-n PD. The obtained photocurrent of the p-i-n PD, $I_{\rm PD}$, is shown in Fig. 5 as a function of the current injected into the DFB laser, $I_{\rm LD}$; the light output from the cleaved facet (the same curve shown in Fig. 4(a)) is also shown, for comparison. The threshold current of the DFB laser observed from the photocurrent characteristic was 0.48 mA, which was the same value measured with the external p-i-n PD. The slope of $I_{\rm LD}$–$I_{\rm PD}$ characteristics was 68.4 μA/mA. $\eta_{\rm d}$ for the p-i-n PD side output can be calculated by assuming the internal quantum efficiency of p-i-n PD of 100% and incorporating the propagation loss of 500-μm-long waveguide of 0.4 dB. The $\eta_{\rm d}$ of the DFB laser was calculated to be 7.5% from the slope of the photocurrent by assuming the p-i-n PD responsivity of 1.25 A/W. The higher wall-plug effi-

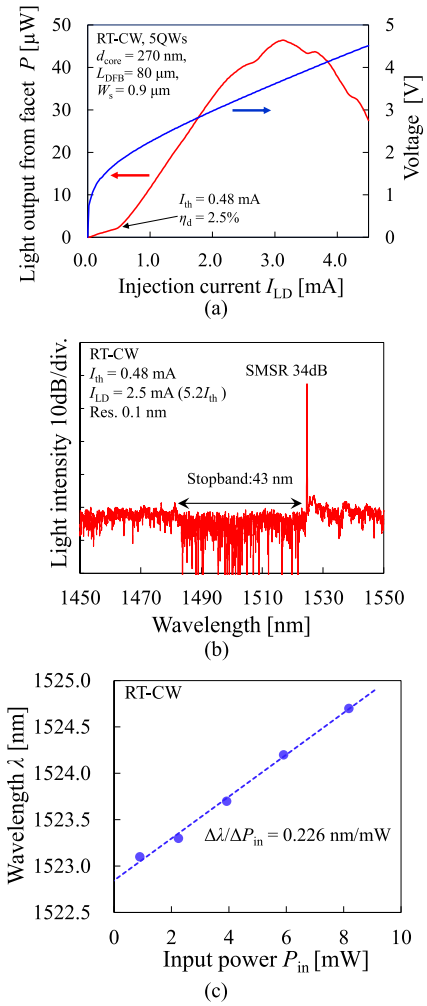

Fig. 4. Lasing characteristics of a membrane DFB laser integrated in an optical link. (a) Light output versus current. (b) Lasing spectrum at a 2.5 mA bias current. (c) Input power versus lasing wavelength characteristics.

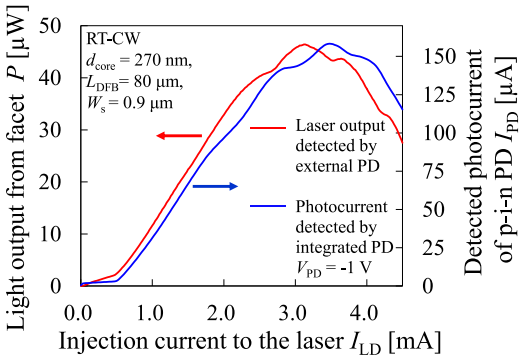

Fig. 5. Photocurrent of the integrated p-i-n PD and light output power of the laser (measured by an external PD) as functions of the laser injection current.

ciency of the laser can be expected by adopting reduced doping concentration of p-InP cladding to reduce the absorption loss. To compensate increased resistivity of p-InP, the distance between the p-side electrode and active stripe region should be as short as possible. Given that the maximum value of I_{PD} was 158 μA at $I_{\mathrm{LD}} = 3.5$ mA, the output power of the DFB laser

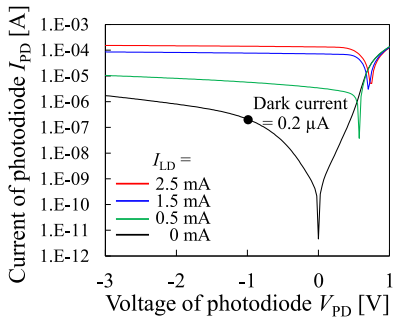

Fig. 6. Current–voltage characteristics of the integrated p-i-n PD, for various injection currents in the DFB laser.

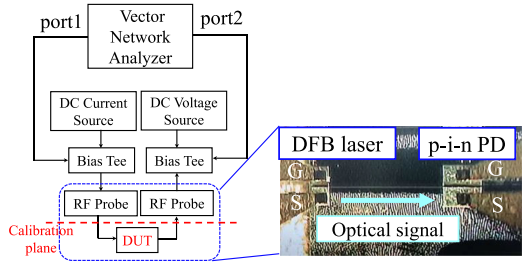

Fig. 7. Setup used to measure the small-signal response of the optical link. The left side image shows the block diagram of the measurement setup. The right side image shows an optical microscopy image of the device under test.

into the integrated waveguide was estimated to be above 126 μW (158 μA ÷ 1.25 A/W), approximately three times higher than that from the cleaved facet (43 μW). This asymmetry in the output ratio was attributed to the facet phase of the grating. Fig. 6 shows the current–voltage characteristics of the integrated p-i-n PD for various laser bias currents, from 0 to 2.5 mA. To avoid a leakage current between the DFB laser and the p-i-n PD, only the curve at a laser current of 0 mA was obtained with opened electrode pads at the DFB laser. As shown, the p-i-n PD dark current was 0.2 μA at a bias voltage of -1 V. The dark current normalized by the absorption area was 1×10^{-1} A/cm^2. This unremarkable dark current density was due either to surface leakage or leakage at the waveguide region. The absorption of p-i-n PD did not reach the saturation region, as can be seen from the fact that the p-i-n PD current in reverse bias conditions was almost independent of the bias voltage.

IV. Small-Signal Modulation Characteristics

The small-signal frequency response S_{21} of the full-optical link was measured with a vector network analyzer (VNA; Anritsu 37397C). The setup for small-signal measurement is depicted in Fig. 7. Ports 1 and 2 of the VNA were connected to bias-tees. A DC source was supplied to each bias-tee. A DC-coupled modulation signal was applied to the DFB laser via a 100-μm-pitch ground-signal (GS) RF probe (Cascade Microtech ACP40). The modulated optical signals were then transmitted via the optical link. The p-i-n PD electrical output was received by a signal-ground probe. The RF component of the detected signal was separated by a bias-tee, and input to Port 2 of the VNA. The measured device chip was put on a heat sink, whose

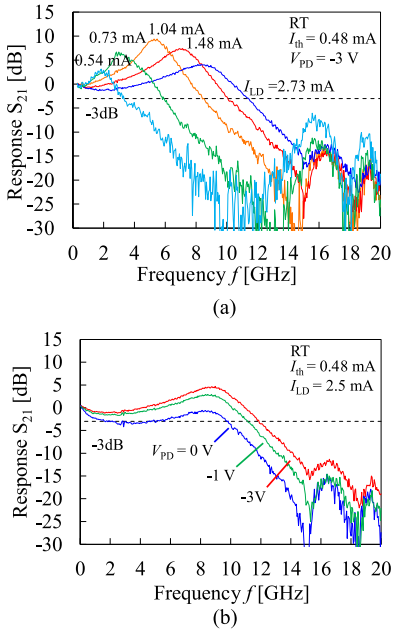

Fig. 8. Small-signal response of the fabricated optical link. (a) Bias current dependence measured at a −3 V PD bias voltage. (b) Bias voltage dependence measured at a 2.5 mA DFB laser bias current.

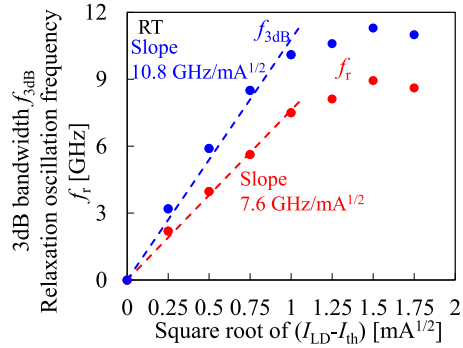

Fig. 9. Relaxation oscillation frequency f_r and 3-dB bandwidth f_{3dB} as a function of the square root of the bias current above threshold.

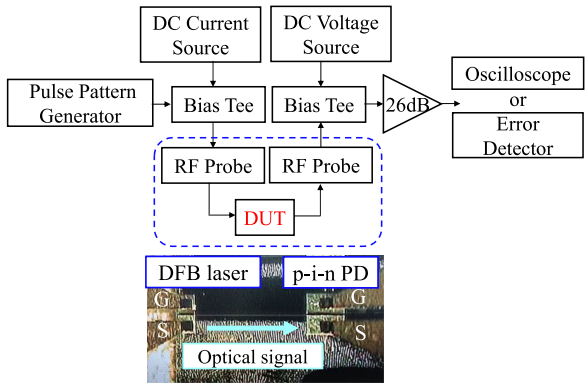

Fig. 10. Measurement setup for evaluation of large-signal transmission through the optical link.

temperature was controlled at 20 °C. In advance of measuring the device, a calibration up to the RF probe tips was performed with an impedance standard substrate (Cascade Microtech, 103-726, GS/SG, up to 67 GHz, pitch: 100 μm–250 μm). Therefore, the contribution of measurement system was excluded from the results.

Fig. 8(a) shows the small-signal frequency response (40 MHz to 20 GHz) of the optical link for various bias currents, with a fixed p-i-n PD bias voltage of −3 V. A clear relaxation oscillation behavior was observed. In addition, the peak frequency increased with the increase in the DFB laser bias current. Therefore, these responses are not electrical crosstalk between probes, but indeed the transmitted optical signal. The 3-dB bandwidth of the optical link was 11.3 GHz at a DFB laser bias current of 2.73 mA. There were bias-current independent peaks near the 16 and 19 GHz frequencies. Although these peaks were due to the electrical signal being transmitted between the RF probes, we believe that the peaks had little effect on the modulation measurement, because the response magnitude was small compared with that of the optical signal. Fig. 8(b) shows the small-signal response for various p-i-n PD bias voltages, for a fixed DFB laser current of 2.5 mA. Increasing the bias voltage enhanced the 3-dB bandwidth, because the electrical field assisted in charge carrier extraction. The maximum bandwidth was obtained at a bias voltage of −3 V. We also determined the modulation efficiency—which is the slope of the relaxation oscillation frequency as a function of the square root of the bias current above threshold—from the small-signal frequency response of the optical link. Fig. 9 shows the 3 dB bandwidth f_{3dB} and the relaxation oscillation frequency f_r as functions of the square root of the bias current above threshold. Because the measurements were performed using on-chip p-i-n PD, f_{3dB} represents bandwidth of the optical link. Modulation efficiencies of 10.8 GHz/mA$^{1/2}$ and 7.6 GHz/mA$^{1/2}$ were obtained for f_{3dB} and f_r, respectively; the latter was smaller than that obtained in our previous work (11 GHz/mA$^{1/2}$) [52]. However, the active volume of the DFB laser in this work was 2.16 μm^3, which was larger than the previous one (0.9 μm^3). Given that the modulation efficiency is proportional to the square root of the active volume, the value of 7.6 GHz/mA$^{1/2}$ for an active volume of 2.16 μm^3 is in good agreement with the previous result.

V. Large-Signal Data-Transmission

Data transmission via the membrane optical link was performed by large-signal direct modulation of the DFB laser. Fig. 10 shows an experimental setup for data-transmission measurements. The electrical modulating signals were generated by a pulse-pattern generator (Anritsu MP1800A, MU181020B, and MU182021A). Electrical signals were sent to the DFB laser via a bias-tee and a GS probe. The optical signal from the DFB laser was transmitted through the passive waveguide, and detected by the p-i-n PD. The electrical output signal of the p-i-n PD was amplified by a 38 GHz electrical amplifier with a 26-dB gain (SHF806E). The signals were recorded with a sampling oscilloscope (Agilent 86109B) or analyzed with an error detector (Anritsu MP1800A, MU181040B, and MU182041A). In this measurement setup, AC components of the p-i-n PD output

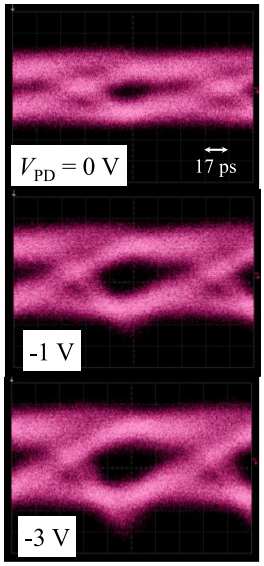

Fig. 11. 10 Gbit/s eye diagrams transmitted through the optical-link for various p-i-n PD bias voltages (0 to −3V). The DFB laser was biased at 2.5 mA, and driven by an NRZ, PRBS (2^{31}-1 signals) electrical modulating signal with a voltage swing of 0.75 V_{pp}.

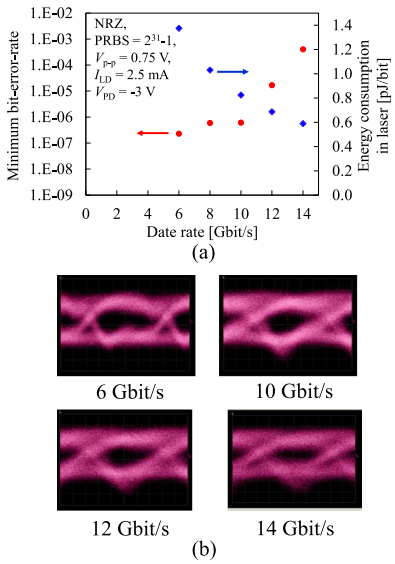

Fig. 12. (a) Bit-error-rate characteristics and energy consumption in the laser of NRZ signal transmission through the membrane optical link; 2.5 mA laser bias current, and −3 V p-i-n PD bias voltage. (b) Eye diagrams for various data rates.

signals were separated from the signals at a bias-tee. Therefore, an extinction ratio of transmitted signal was not obtained.

The input electrical signal to the DFB laser was a non-return-to-zero (NRZ) pseudorandom binary sequence (PRBS) of 2^{31}-1 signals, with a voltage swing of 0.75 V_{pp}. Fig. 11 shows transmitted 10 Gbit/s eye diagrams at a 2.5 mA DFB laser bias current, recorded for various p-i-n PD bias voltages. As the bias voltage of the p-i-n PD increased, larger eye openings were observed, which is consistent with the results of the small-signal measurements. Fig. 12(a) shows the measured bit-error-rate (BER) versus the data-rate and the energy consumption in the laser at each data-rate. All plots were obtained in the same operating conditions (except for the data-rate). A BER in the order of 10^{-7} was obtained up to a data rate of 10 Gbit/s. A energy consumption of the laser at 10 Gbit/s was 0.825 pJ/bit. Above 10 Gbit/s, the BER rapidly degraded. The eye diagrams corresponding to the measured BER plots are shown in Fig. 12(b); as shown, the eye diagrams for 12 and 14 Gbit/s are more closed, because of signal distortion.

VI. Conclusion

We described a monolithically integrated membrane optical link fabricated on a Si substrate, which employs a membrane DFB laser and a p-i-n PD. The integrated DFB laser showed a threshold current of 0.48 mA, with a sub-mode suppression ratio of 34 dB at a bias current of 2.5 mA. The integrated p-i-n PD detection of the transmitted light output of the DFB laser was confirmed from static measurements of the optical link. The dynamic characteristics of the membrane optical link were obtained for both small-signal and large-signal modulations. For a DFB laser bias current of 2.73 mA and a p-i-n PD bias voltage of −3 V, the obtained 3-dB bandwidth of the optical link was 11.3 GHz. Data-transmission with NRZ PRBS of 2^{31}-1 signals was performed. 10 Gbit/s transmission with a BER of 6×10^{-7} was achieved at a DFB laser bias current of 2.5 mA. The obtained results show that optical links using a membrane DFB laser are attractive candidates for on-chip optical interconnections.

Acknowledgment

The authors would like to thank Professors S. Akiba, T. Mizumoto, M. Asada, Y. Miyamoto, M. Watanabe, Y. Shoji, and S. Suzuki of the Tokyo Institute of Technology for the fruitful discussions.

References

[1] R. Ho, K. Mai, and M. Horowitz, "The future of wires," *Proc. IEEE*, vol. 89, no. 4, pp. 490–504, Apr. 2001
[2] K. Banerjee and A. Mehrotra, "Global (interconnect) warming," *IEEE Circuits Devices Mag.*, vol. 17, no. 5, pp. 16–32, Sep. 2001.
[3] S. Borkar and A. A. Chien, "The future of microprocessors," *Commun. ACM*, vol. 54, no. 5, pp. 67–77, May 2011.
[4] N. Srivastava, H. Li, F. Kreupl, and K. Banerjee, "On the applicability of single-walled carbon nanotubes as VLSI interconnects," *IEEE Trans. Nanotechnol.*, vol. 8, no. 4, pp. 542–559, Jul. 2009.
[5] A. P. Jose, G. Patounakis, and K. L. Shepard, "Pulsed current-mode signaling for nearly speed-of-light intrachip communication," *IEEE J. Solid-State Circuits*, vol. 41, no. 4, pp. 772–780, Apr. 2006.
[6] E. Mensink, D. Schinkel, E. Klumperink, E. van Tuijl, and B. Nauta, "A 0.28pJ/b 2Gb/s/ch transceiver in 90 nm CMOS for 10 mm on-chip interconnects," in *Proc. IEEE Int. Solid-State Circuits Conf. Dig. Tech. Papers*, Feb. 2007, pp. 414–415.
[7] T. Maekawa, H. Ito, and K. Masu, "An 8Gbps 2.5mW on-chip pulsed-current-mode transmission line interconnect with a stacked-switch Tx," in *Proc. 34th Eur. Solid-State Circuits Conf. Dig. Tech. Papers*, Sep. 2008, pp. 474–477.
[8] D. A. B. Miller, "Rationale and challenges for optical interconnects to electronic chips," *Proc. IEEE*, vol. 88, no. 6, pp. 728–749, Jun. 2000.
[9] G. Chen *et al.*, "Prediction of CMOS compatible on-chip optical interconnect," *Integr. VLSI J.*, vol. 40, no. 4, pp. 434–446, Jul. 2007.
[10] K. Ohashi *et al.*, "On-chip optical interconnect," *Proc. IEEE*, vol. 97, no. 7, pp. 1186–1198, Jul. 2009.

[11] N. Ophir *et al.*, "First demonstration of error-free operation of a full silicon on-chip photonic link," in *Proc. Opt. Fiber Commun. Conf.*, Los Angeles, CA, USA, 2011, Paper OWZ3.

[12] X. Xiao *et al.*, "High-speed on-chip photonic link based on ultralow-power microring modulator," in *Proc. Opt. Fiber Commun. Conf.*, San Francisco, CA, USA, 2014, Paper Tu2E.6.

[13] E. Timurdogan *et al.*, "An ultra low power 3D integrated intra-chip silicon electronic-photonic link," in *Proc. Opt. Fiber Commun. Conf.*, Los Angeles, CA, USA, 2015, Paper Th5B.8.

[14] C. Sun *et al.*, "Single-chip microprocessor that communicates directly using light," *Nature*, vol. 528, pp. 534–538, Dec. 2015.

[15] E. Timurdogan *et al.*, "An ultralow power athermal silicon modulator," *Nature Commun.*, vol. 5, pp. 1–11, Jun. 2014.

[16] K. Chen *et al.*, "Wavelength-multiplexed duplex transceiver based on III-V/Si hybrid integration for off-chip and on-chip optical interconnects," *IEEE Photon. J.*, vol. 8, no. 1, Feb. 2016, Art. no. 7900910.

[17] J. J. G. M. van der Tol *et al.*, "Photonic integration on an InP-membrane," in *Proc. Adv. Photon.*, Vancouver, Canada, 2016, Paper ITu2A.1.

[18] D. A. B. Miller, "Device requirements of optical interconnects to silicon chips," *Proc. IEEE*, vol. 97, no. 7, pp. 1166–1185, Jul. 2009.

[19] P. Moser *et al.*, "81 fJ/bit energy-to-data ratio of 850 nm vertical-cavity surface emitting lasers for optical interconnects," *Appl. Phys. Lett.*, vol. 98, no. 23, Jun. 2011, Art. no. 231106.

[20] S. Imai *et al.*, "Recorded low power dissipation in highly reliable 1060-nm VCSELs for 'green' optical interconnection," *IEEE J. Sel. Topics Quantum Electron.*, vol. 17, no. 6, pp. 1614–1620, Nov. 2011.

[21] P. Shen *et al.*, "Chip-level optical interconnects using polymer waveguide integrated with laser/PD on silicon," *IEEE Photon. Technol. Lett.*, vol. 27, no. 13, pp. 1359–1362, Jul. 2015.

[22] K. Ohira *et al.*, "High-speed and stable operation of highly unidirectional III-V/silicon microring lasers for on-chip optical interconnects," in *Proc. Conf. Lasers Electro-Opt. Conf.*, San Jose, CA, USA, 2015, Paper STu2F.3.

[23] J. Van Campenhout *et al.*, "Low-footprint optical interconnect on an SOI chip through heterogeneous integration of InP-based microdisk lasers and microdetectors," *IEEE Photon. Technol. Lett.*, vol. 21, no. 8, pp. 522–524, Apr. 2009.

[24] T. Spuesens, J. Bauwelinck, P. Regreny, and D. Van Thourhout, "Realization of a compact optical interconnect on silicon by heterogeneous integration of III-V," *IEEE Photon. Technol. Lett.*, vol. 25, no. 14, pp. 1332–1335, Jul. 2013.

[25] K. Takeda *et al.*, "Few-fJ/bit data transmissions using directly modulated lambda-scale embedded active region photonic-crystal lasers," *Nature Photon.*, vol. 7, no. 7, pp. 569–575, May 2013.

[26] T. Sato *et al.*, "Photonic crystal lasers for chip-to-chip and on-chip optical interconnects," *IEEE J. Sel. Topics Quantum Electron.*, vol. 21, no. 6, Nov./Dec. 2015, Art. no. 4900410.

[27] S. Arai, N. Nishiyama, T. Maruyama, and T. Okumura, "GaInAsP/InP membrane lasers for optical interconnects," *IEEE J. Sel. Topics Quantum Electron.*, vol. 17, no. 5, pp. 1381–1389, Sep./Oct. 2011.

[28] R. Nagarajan *et al.*, "InP photonic integrated circuits," *IEEE J. Sel. Topics Quantum Electron.*, vol. 16, no. 5, pp. 1113–1125, Sep./Oct. 2010.

[29] J. Summers *et al.*, "40 channels×57 Gb/s monolithically integrated inP-based coherent photonic transmitter," in *Proc. 40th Eur. Conf. Opt. Commun.*, Cannes, France, 2014, Paper 2.5.

[30] T. Tadokoro *et al.*, "Operation of a 25-Gb/s direct modulation ridge waveguide MQW-DFB laser up to 85 °C," *IEEE Photon. Technol. Lett.*, vol. 21, no. 16, pp. 1154–1156, Aug. 2009.

[31] M. Matsuda *et al.*, "Uncooled low-driving-current 25.8 Gbit/s direct modulation using 1.3 μm AlGaInAs MQW distributed-reflector lasers," *Electron. Lett.*, vol. 48, no. 8, pp. 450–452, Apr. 2012.

[32] T. Okumura, T. Koguchi, H. Ito, N. Nishiyama, and S. Arai, "Injection-type GaInAsP/InP membrane buried heterostructure distributed feedback laser with wirelike active regions," *Appl. Phys. Express*, vol. 4, no. 4, Mar. 2011, Art. no. 042101.

[33] S. Sakamoto *et al.*, "Strongly index-coupled membrane BH-DFB lasers with surface corrugation grating," *IEEE J. Sel. Topics Quantum Electron.*, vol. 13, no. 5, pp. 1135–1141, Sep./Oct. 2007.

[34] T. Hiratani *et al.*, "Energy cost analysis of membrane distributed-reflector lasers for on-chip optical interconnects," *IEEE J. Sel. Topics Quantum Electron.*, vol. 21, no. 6, pp. 299–308, Nov./Dec. 2015.

[35] T. Okamoto, N. Nunoya, Y. Onodera, S. Tamura, and S. Arai, "Continuous wave operation of optically pumped membrane DFB laser," *Electron. Lett.*, vol. 37, no. 24, pp. 1455–1457, Nov. 2001.

[36] T. Okamoto *et al.*, "Optically pumped membrane BH-DFB lasers for low-threshold and single-mode operation," *IEEE J. Sel. Topics Quantum Electron.*, vol. 9, no. 5, pp. 1361–1366, Sep./Oct. 2003.

[37] S. Sakamoto, T. Okamoto, T. Yamazaki, S. Tamura, and S. Arai, "Multiple-wavelengths membrane BH-DFB laser arrays," *IEEE J. Sel. Topics Quantum Electron.*, vol. 11, no. 5, pp. 1174–1179, Sep./Oct. 2005.

[38] K. Oe, Y. Noguchi, and C. Caneau, "GaInAsP lateral current injection lasers on semi-insulating substrates," *IEEE Photon. Technol. Lett.*, vol. 6, no. 4, pp. 479–481, Apr. 1994.

[39] T. Okumura *et al.*, "Lateral current injection GaInAsP/InP laser on semi-insulating substrate for membrane-based photonic circuits," *Opt. Express*, vol. 17, no. 15, pp. 12564–12570, Jul. 2009.

[40] T. Shindo *et al.*, "GaInAsP/InP lateral-current-injection distributed feedback laser with a-Si surface grating," *Opt. Express*, vol. 19, no. 3, pp. 1884–1891, Jan. 2011.

[41] T. Shindo *et al.*, "Lateral-current-injection distributed feedback laser with surface grating structure," *IEEE J. Sel. Topics Quantum Electron.*, vol. 17, no. 5, pp. 1175–1182, Sep. 2011.

[42] T. Shindo *et al.*, "Lateral-current-injection type membrane DFB laser with surface grating," *IEEE Photon. Technol. Lett.*, vol. 25, no. 13, pp. 1282–1285, Jul. 2013.

[43] D. Inoue *et al.*, "Room-temperature continuous-wave operation of GaInAsP/InP lateral-current-injection membrane laser bonded on Si substrate," *Appl. Phys. Express*, vol. 7, no. 7, Jun. 2014, Art. no. 072701.

[44] T. Hiratani *et al.*, "Thermal properties of lateral-current-injection semiconductor membrane Fabry–Perot laser under continuous-wave operation," *Jpn. J. Appl. Phys.*, vol. 54, no. 4, Mar. 2015, Art. no. 042701.

[45] Y. Abe, K. Kishino, Y. Suematsu, and S. Arai, "GaInAsP/InP integrated laser with butt-jointed built-in distributed-Bragg-reflection waveguide," *Electron. Lett.*, vol. 17, no. 25, pp. 945–947, Dec. 1981.

[46] E. J. Skogen, J. S. Barton, S. P. Denbaars, and L. A. Coldren, "A quantum-well-intermixing process for wavelength-agile photonic integrated circuits," *IEEE J. Sel. Topics Quantum Electron.*, vol. 8, no. 4, pp. 863–869, Jul./Aug. 2002.

[47] B. Mason, S. P. Denbaars, and L. A. Coldren, "Tunable sampled-grating DBR lasers with integrated wavelength monitors," *IEEE Photon. Technol. Lett.*, vol. 10, no. 8, pp. 1085–1087, Aug. 1988.

[48] D. Inoue *et al.*, "Butt-joint built-in (BJB) structure for membrane photonic integration," in *Proc. 25th Int. Conf. Indium Phosphide Related Mater.*, Kobe, Japan, 2013, Paper TuD3-6.

[49] D. Inoue *et al.*, "Sub-milliampere threshold operation of butt-jointed built-in membrane DFB laser bonded on Si substrate," *Opt. Express*, vol. 23, no. 6, pp. 7771–7778, Mar. 2015.

[50] T. Hiratani *et al.*, "Room-temperature continuous-wave operation of membrane distributed-reflector laser," *Appl. Phys. Express*, vol. 8, no. 11, Oct. 2015, Art. no. 112701.

[51] D. Inoue *et al.*, "High-modulation efficiency operation of GaInAsP/InP membrane distributed feedback laser on Si substrate," *Opt. Express*, vol. 23, no. 22, pp. 29024–29031, Nov. 2015.

[52] D. Inoue *et al.*, "Low-bias current 10 Gbit/s direct modulation of GaInAsP/InP membrane DFB laser on silicon," *Opt. Express*, vol. 24, no. 16, pp. 18571–18579, Aug. 2016.

[53] D. Inoue *et al.*, "Monolithic integration of membrane-based butt-jointed built-in DFB Lasers and p-i-n photodiodes bonded on Si substrate," *IEEE J. Sel. Topics Quantum Electron.*, vol. 21, no. 6, pp. 392–398, Nov./Dec. 2015.

Daisuke Inoue (S'16) was born in Okayama Prefecture, Japan, in 1990. He received the B.E. and M.E. degrees in electrical and electronic engineering in 2013 and 2015, respectively, from the Tokyo Institute of Technology, Tokyo, Japan, where he is currently working toward the Ph.D. degree in electrical and electronic engineering.

His current research interest focuses on membrane-based photonic devices for optical interconnection.

Mr. Inoue is a student member of the Institute of Electronics, Information and Communication Engineers and the Japan Society of Applied Physics. He received the CSW2016 Best Student Paper Award.

Takuo Hiratani (S'13) was born in Ishikawa Prefecture, Japan, in 1990. He received the B.E. degree in electrical and electronic engineering from Kanazawa University, Ishikawa, Japan, in 2012, and the M.E. degree in electrical and electronic engineering in 2014 from the Tokyo Institute of Technology, Tokyo, Japan, where he is currently working toward the Ph.D. degree in electrical and electronic engineering.

His current research interest focuses on membrane-based photonic devices for on-chip optical interconnection.

Mr. Hiratani is a student member of the Institute of Electronics, Information and Communication Engineers and the Japan Society of Applied Physics.

Kai Fukuda was born in Toyama Prefecture, Japan, in 1990. He received the B.E. degree in electrical and electronic engineering in 2015 from the Tokyo Institute of Technology, Tokyo, Japan, where is currently working toward the M.E. degree in the Department of Electrical and Electronic Engineering.

His current research interest focuses on membrane-based DFB lasers for optical interconnection.

Mr. Fukuda is a student member of the Japan Society of Applied Physics.

Takahiro Tomiyasu was born in Fukuoka Prefecture, Japan, in 1992. He received the B.E. degree in electrical and electronic engineering in 2015 from the Tokyo Institute of Technology, Tokyo, Japan, and is currently working toward the M.E. degree in the Department of Electrical and Electronic Engineering.

His current research interest focuses on membrane-based DFB lasers for optical interconnection.

Mr. Tomiyasu is a student member of the Institute of Electronics, Information, and Communication Engineers.

Zhichen Gu was born in Shanghai, China, in 1991. He received the B.E. degree in communications engineering from Donghua University, Shanghai, China, in 2012, and the M.E. degree in electrical and electronic engineering in 2015 from the Tokyo Institute of Technology, Tokyo, Japan, where he is currently working toward the Ph.D. degree in the Department of Electrical and Electronic Engineering.

His current research interest focuses on membrane-based photonic devices for optical interconnection.

Mr. Gu is a student member of the Institute of Electronics, Information and Communication Engineers and the Japan Society of Applied Physics.

Tomohiro Amemiya (S'06–M'09) was born in Tokyo, Japan, in 1981. He received the B.S., M.S., and Ph.D. degrees in electronic engineering from the University of Tokyo, Tokyo, Japan, in 2004, 2006, and 2009, respectively.

In 2009, he moved to the Quantum Electronics Research Center, Tokyo Institute of Technology, Tokyo, Japan, as an Assistant Professor. Since 2016, he has been an Assistant Professor in the Institute of Innovative Research, Tokyo Institute of Technology. His research interests include physics of photonic integrated circuits, metamaterials for optical frequencies, semiconductor light-controlling devices, and the technologies for fabricating these devices.

Dr. Amemiya is a member of the Optical Society of America, the American Physical Society, and the Japan Society of Applied Physics. He received the 2007 IEEE Photonics Society Annual Student Paper Award, the 2008 IEEE Photonics Society Graduate Student Fellowships, the 2012 Konica Minolta Imaging Award, the 2015 Yazaki Memorial Foundation Award, and the 2016 Young Scientists' Prize of the Commendation for Science and Technology by the Minister of Education, Culture, Sports, Science and Technology.

Nobuhiko Nishiyama (M'01–SM'07) was born in Yamaguchi Prefecture, Japan, in 1974. He received the B.E., M.E., and Ph.D. degrees from the Tokyo Institute of Technology, Tokyo, Japan, in 1997, 1999, and 2001, respectively. During his Ph.D. work, he demonstrated single-mode 0.98- and 1.1-μm VCSEL arrays with stable polarization using misoriented substrates for high-speed optical networks and MOCVD-grown GaInNAs VCSELs.

He joined Corning, Inc., New York, in 2001, and worked with the Semiconductor Technology Research Group. At Corning, he worked on several subjects, including short-wavelength lasers, 1060-nm DFB/DBR lasers, and long-wavelength InP-based VCSELs. Since 2006, he has been an Associate Professor with the Tokyo Institute of Technology. His current main research interests include transistor lasers, silicon photonics, III–V silicon hybrid optical devices, and terahertz-optical signal conversions involving optics–electronics–radio integration circuits.

Dr. Nishiyama is a member of the Japan Society of Applied Physics and the Institute of Electronics, Information and Communication Engineers (IEICE). He received the Excellent Paper Award from the IEICE of Japan in 2001, the Young Scientists' Prize of the Commendation for Science and Technology from the Minister of Education, Culture, Sports, Science and Technology in 2009, and the Ichimura Prize in Science for Distinguished Achievement in 2016.

Shigehisa Arai (M'83–SM'06–F'10) was born in Kanagawa Prefecture, Japan, in 1953. He received the B.E., M.E., and D.E. degrees in electronics from the Tokyo Institute of Technology, Tokyo, Japan, in 1977, 1979, and 1982, respectively. During his Ph.D. work, he demonstrated room-temperature CW operations of 1.11–1.67 μm long-wavelength lasers fabricated by liquid-phase epitaxy, as well as their single-mode operations under rapid direct modulation.

He joined the Department of Physical Electronics, Tokyo Institute of Technology, as a Research Associate in 1982, and joined AT&T Bell Laboratories, Holmdel, NJ, as a Visiting Researcher from 1983 to 1984, on leave from the Tokyo Institute of Technology. He further became a Lecturer in 1984, an Associate Professor in 1987, and a Professor in the Research Center for Quantum Effect Electronics and the Department of Electrical and Electronic Engineering in 1994. Since 2004, he has been a Professor in the Quantum Nanoelectronics Research Center, Tokyo Institute of Technology. His research interests include photonic integrated devices such as dynamic-single-mode and wavelength-tunable semiconductor lasers, semiconductor optical amplifiers, and optical switches/modulators. His current research interests include studies of low-damage and cost-effective processing technologies of ultrafine structures for high-performance lasers and photonic integrated circuits on silicon platforms.

Dr. Arai is a member of the Optical Society of America, the Institute of Electronics, Information and Communication Engineers (IEICE), and the Japan Society of Applied Physics (JSAP). He received the Excellent Paper Award from the IEICE of Japan in 1988, the Michael Lunn Memorial Award from the Indium Phosphide and Related Materials Conference in 2000, Prizes for Science and Technology of the Commendation for Science and Technology from the Minister of Education, Culture, Sports, Science and Technology in 2008, an Electronics Society Award and the Achievement Award from IEICE in 2008 and 2011, respectively, a JSAP Fellowship in 2008, and the SSDM Award from the International Conference on Solid-State Devices and Materials in 2016.